Mixed Norm Wavelet Estimation for Residual Deconvolution

Carlos A. Cunha (Petrobras S.A.)

This paper was prepared for presentation at the 15^{th} International Congress of The Brazilian Geophysical Society held in Rio de Janeiro, Brazil, July 31 to August 3, 2017.

Abstract

We address here the problem of estimating the time and space varying residual wavelet to be used in a broadband reflectivity inversion algorithm. The usual form of wavelet estimation uses a L_2 norm inversion algorithm, which have some limitations when few relevant reflection events are present within a specific time window. We propose the use of an alternative modified L_1 norm to obtain a more robust estimation of the residual seismic pulse. The robustness of the method is illustrated with synthetic and field data examples.

Introduction

Ideally, the ultimate goal of routine seismic processing/imaging is to obtain a set of amplitude volumes, where the amplitude of a given sample in each volume corresponds to the P wave reflection coefficiente at that subsurface position for a given angle of incidence. Several steps of the seismic processing flow aim to compensate for the effects on the amplitude and phase spectra of the seismic wavelet caused during its generation, recording and propagation through the sub-surface. Ideally, these steps should lead the effective seismic pulse to approach a unit impulse.

Despite all these steps, which include debbubling, ghost removal and compensation for absortion, a residual wavelet will always be present in the final image volumes, which imposes limits for the resolution of the geological layers. One of the forms of broadening the spectrum, in order to increase the resolution of the images, is to apply a zero phase deconvolution to the seismic volumes.

Wavelet estimation is an important part of the deconvolution process (Portniaguine and Castagna, 2005), and has been the subject of recent research related to the improvement of seismic resolution (Zhou et. al., 2016).

Our goal is to estimate the time and space varying residual zero-phase wavelet to be used in a sparse-oriented deconvolution algorithm used in Petrobras (Rosa, 2010). The standard form of wavelet estimation uses a L_2 norm inversion algorithm, which have some limitations when few relevant reflection events are present within a specific time window. To illustrate these limitations, we use as a reference throughout the paper the synthetic data corresponding to a wedge model, as shown in Figure 1-a.

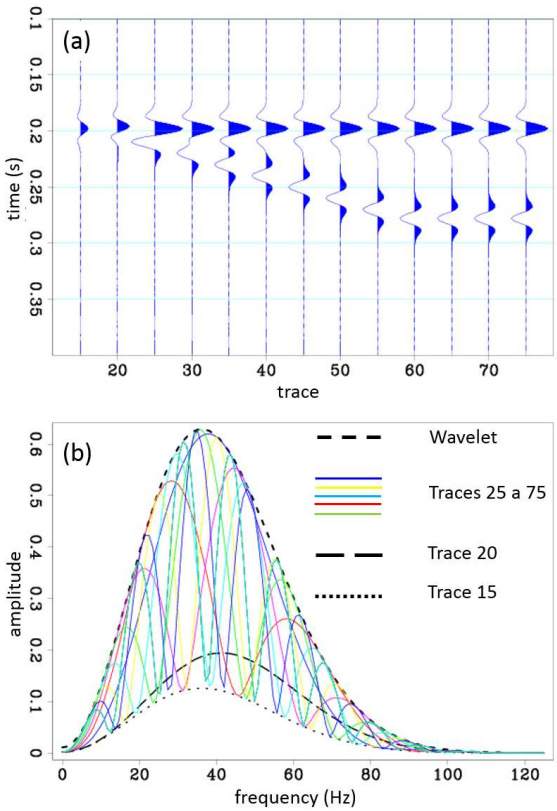

Figure 1: (a) Sinthetic data for a wedge model; (b) amplitude spectra for the traces in (a). Trace 15, corresponds to a single interface (with less impedance contrast) while trace 20 shows a tunning effect associated with the two relections.

Figure 1-b presents the spectra of the traces from 1-a. The spectrum of each individual trace shows a particular pattern of ressonant frequencies, which relates to the time delay between the top and bottom reflections of the wedge. An importatnt property represented in the figure is that all the individual spectra share the same envelope, which is the spectrum of the original pulse.
As we will show in the next sessions, a modified L_1 norm is more suitable for a robust estimation of the residual seismic pulse, than the usual L_2 norm.

L_2 norm wavelet estimation

The first step involves the transformation of the spectrum $S(\omega)$ in the function $Y(\omega)$, which in the discrete formulation is given by

$$Y_j = \ln \frac{S_j}{\omega_j^{\alpha}}, \tag{1}$$

where S_j corresponds to the amplitude spectrum, ω_j, is the frequency, and α is a positive exponent smaller than one.
An usual way to formulate the problem of wavelet estimation for a time window with transformed spectrum defined by Y_j is to obtain the coefficients a_i that defines the polynomial P_j of degree N (Rosa and Ulrych, 1991):

$$P_j = \sum_{i=1}^{N} a_i \omega_j^i \tag{2}$$

which minimizes the L_2 norm error function

$$E_2 = \sum_{j=1}^{M} |Y_j - P_j|^2. \tag{3}$$

The solution is given by solving for the coefficients $(a_1, a_2, ..., a_N)$, the set of linear equations

$$\frac{\partial E_2(a_1, a_2, ..., a_N)}{\partial a_k} = 0, \quad \text{for} \quad k\{1, N\} \tag{4}$$

which leads to

$$\sum_i \sum_j \omega_j^{i+k} a_i = \sum_j Y_j \omega_j^k \tag{5}$$

The wavelets estimated with the L_2 norm (Equation 5), for 4 selected traces from Figure 1-a, are presented in Figure 2. The limitations of the L_2 solution to retrieve the true wavelet become apparent from this figure.

Modified L_1 norm wavelet estimation

In order to improve the pulse estimation, let's first analyse the residuals represented in Equation 3. Figure 3-a shows, for trace 50, the transformed spectrum Y_j, and the polinomial solution P_j, and 3-b the L_2 residuals before squaring (that is, the L_1 residuals) for the solution. In order to achieve the goal of the solution P_j to approach the envelope of Y_j we should have an error function that penalizes only the positive part of $Y_j - P_j$ in Figure 3-b.
Following this reasoning, we present Equation 6 as a first attempt to define an error function whose minimization would lead to the envelope of the trace spectrum as the solution.

$$E_1^+ = \sum_{j=1}^{M} \{(Y_j - P_j) + |Y_j - P_j|\}. \tag{6}$$

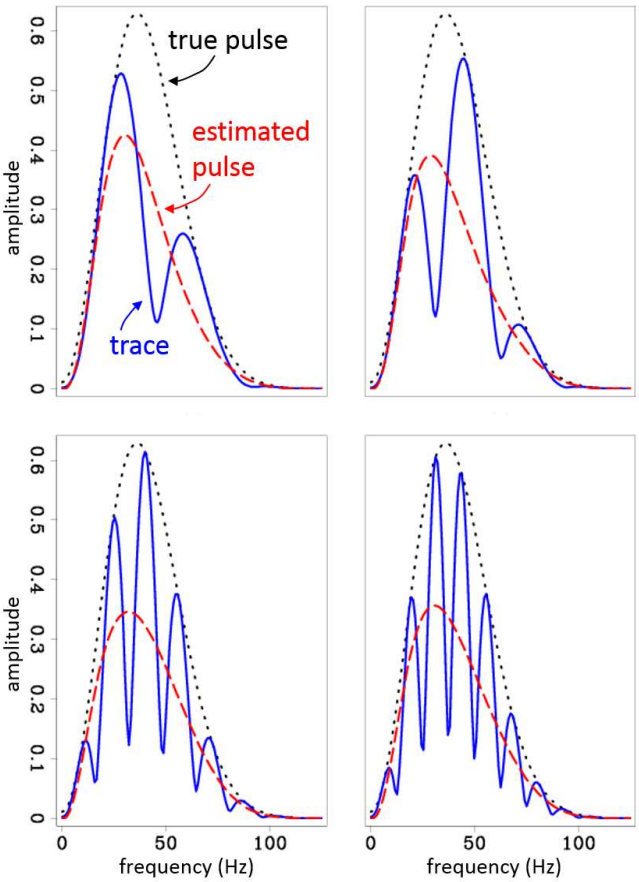

Figure 2: L_2 norm estimation results for 4 traces from Figure 1. The traces are: 30 (top left), 35 (top right), 50 (bottom left), 60 (bottom right).

As we will discuss later in this paper, the solution of this equation is achieved by an iterative inversion algorithm. The residuals represented in Equation 6, for

the specific case of the L_2 solution for trace 50 are depicted in Figure 4.

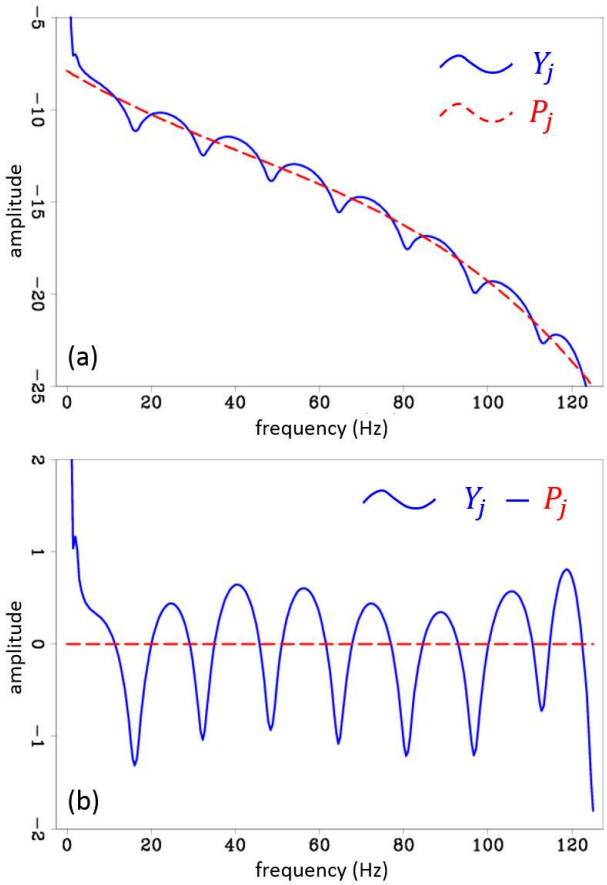

Figure 3: (a) Transformed spectrum Y_j and the L_2 norm solution for the fitting polynomial P_j; (b) Residuals for the L_2 norm solution.

Although the solution of Equation 6 converges to the desired envelope for low order polinomials (up to 4^{th} order), it becomes unstable for higher order, as illustrated in Figure 5. The evolution with iteration of the residuals are shown in 5-a, while the evolution of the solution is shown in 5-b. Although the first iterations show convergence to the desired solution, the next iterations diverge. The reason is that the error function, as defined by Equation 6, becomes zero for all polinomial functions that have no intersection with the transformed spectrum. The envelope is just one of these functions.

In order to avoid solutions that diverge from the desired envelope, we must introduce another term in the objective function, that penalizes the negative residuals, but in a smaller scale than the positive residuals. We define thus a new error function:

$$E_1^{\pm} = \sum_{j=1}^{M} \{[(Y_j - P_j) + |Y_j - P_j|] - \beta\,[(Y_j - P_j) - |Y_j - P_j|]\}\,,$$

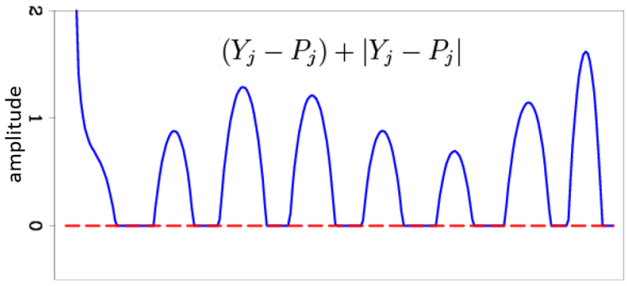

Figure 4: Residuals for the objective function defined by equation 6, for the same functions Y_j and P_j used in Figure 3.

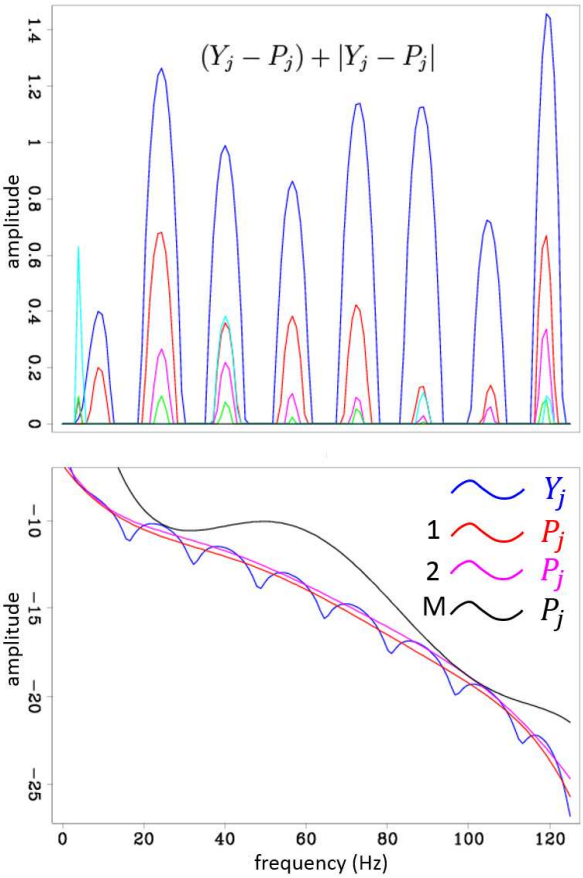

Figure 5: (a) Evolution with iteration, of the residuals for the E_{1+} solution; (b) evolution with iteration of the fitting function P_j for the E_{1+} solution.

where β is a scalar smaller than one. After regrouping the terms

$$E_1^{\pm} = \sum_{j=1}^{M} \{(1-\beta)(Y_j - P_j) + (1+\beta)|Y_j - P_j|\}. \quad (7)$$

The residuals represented in Equation 7, for the specific case of the L_2 solution for trace 50 are depicted in Figure 6. If we compare with Figure 4, we can see that the negative residuals are now present with a small weight.

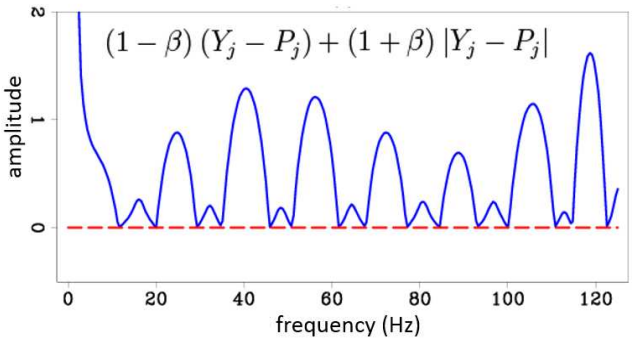

Figure 6: Residuals for the objective function defined by Equation 7.

Representing the absolute value $|Y_j - P_j|$ by $\sqrt{(Y_j - P_j)^2}$ we can apply equation 4 to $E_1^{\pm}$ and obtain the folowing set of equations for $k = 1, 2, ..., N$.

$$\sum_i (1+\beta) \sum_j \frac{\omega_j^{i+k}}{\sqrt{\left(Y_j - \sum_i a_i \omega_j^i\right)^2}} a_i =$$
$$(1+\beta) \sum_j \frac{Y_j \omega_j^k}{\sqrt{\left(Y_j - \sum_i a_i \omega_j^i\right)^2}} + (1-\beta) \sum_j (-\omega_j^k).$$

These set of non-linear equations should be solved for the unknown coefficients a_i. Linearization is achieved using Iterative Reweighted Least Squares (IRLS), which for iteration $m \geq 2$ leads to the following set of equations:

$$\sum_i \sum_j \frac{\omega_j^{i+k}}{\sqrt{\left(Y_j - \sum_i a_i^{(m-1)} \omega_j^i\right)^2 + \epsilon}} a_i^{(m)} =$$
$$\sum_j \frac{Y_j}{\sqrt{\left(Y_j - \sum_i a_i^{(m-1)} \omega_j^i\right)^2 + \epsilon}} - \frac{(1-\beta^m)}{(1+\beta^m)} \sum_j \omega_j^k, \quad (8)$$

which, for the specific case of, $m = 1$ reduces to the norm 2 solution given by Equation 5.

In Equation 8 β^m is an iteration dependent coefficient, that decreases at a specified rate as the iterations proceed. The initial value must be smaller than one.

Figure 7 shows the evolution of the residuals, as well as the evolution of the solution for a polinomial of 6^{th} order. The wavelets estimated with

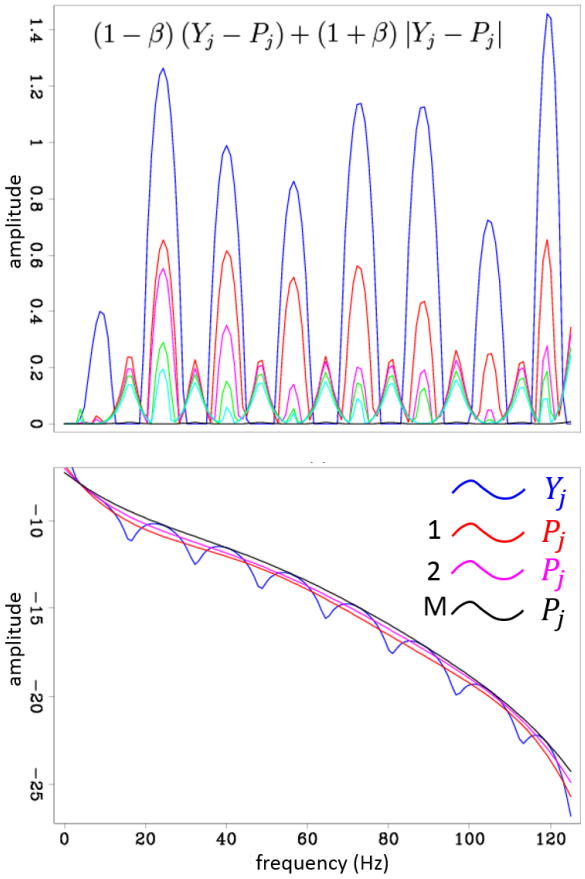

Figure 7: (a) Evolution with iteration, of the residuals for the E_1^{+-} solution; (b) evolution with iteration of the fitting function P_j for the E_1^{+-} solution.

the modified L_1 norm (using the iterative solution of quation 8) for the same 4 traces used in Figure 2 are presented in Figure 8. The wavelets estimated with the modified L_1 norm are clearly superior to retrieve the true seismic pulse when compared to the ones estimated with the L_2 norm.

Examples

The first example refers to the same wedge model, used throughout the paper to illustrate the concepts that support the proposed form for the modified L_1 norm. We applied the wavelet estimation inversion for all traces, followed by the reflectivity inversion.

The results are presented in Figure 9. The retrieved reflectivity using the L_1 norm wavelets are less contaminated by artifacts when compared to the reflectivity obtained with the L_2 norm wavelets. The

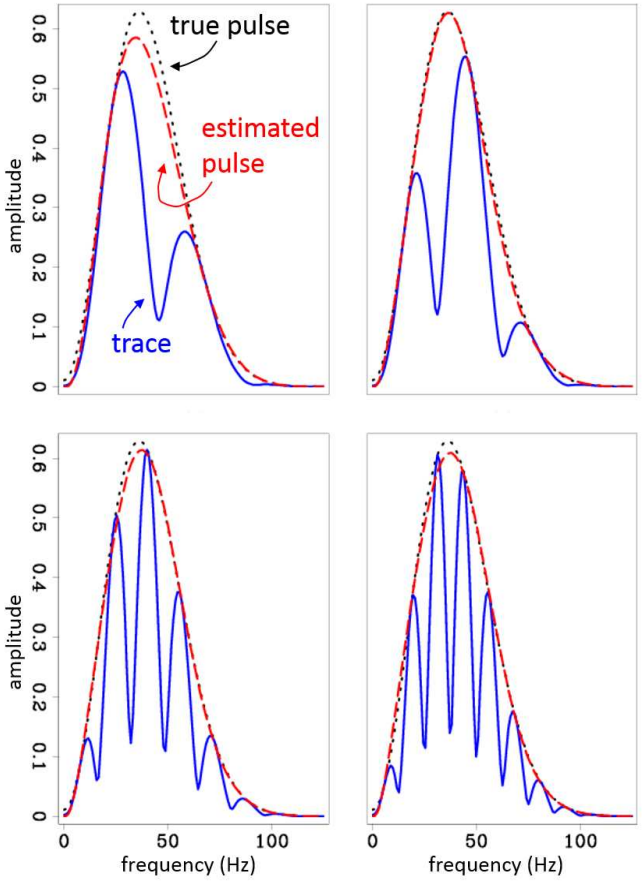

Figure 8: Modified L_1 norm estimation results for 4 traces from Figure 1. The traces are: 30 (top left), 35 (top right), 50 (bottom left), 60 (bottom right).

differences between the L_2 and the modified L_1 norm estimates become more clear when we compare the integrated reflectitvities, which correspond to a band-limited version of the acoustic impedance. Figure 10 shows the impedances from the two reflectivity panels of Figure 9 (one for each norm), as well as the impedance from the reflectivity inversion using the true wavelet. The modified L_1 result is almost identical to the one with the correct wavelet.

The second example involves the application of the modified L_1 norm to a field data from Santos basin (Brazil). A reflectivity inversion process was applied to generate band-limited impedance data. Figure 11-a shows the amplitude data, while 11-b and 11-c, show the band-limited impedance using the L_2 and L_1 norm respectively. The increase in resolution with the L_1 norm is clear from the figure. Although no spectral balancing algorithm have been applied in the process, the improvement achieved with the L_1 norm can be related to the better spectral homogeneity present in it's inverted reflectivity, as demonstrated by Figure 12.

Conclusions

Wavelet estimation plays an inportant role in the process of reflectivity inversion from band-limited seismic data. The process, considering zero-phase wavelets, is usually based on a smoothed version of the spectrum of the seismic trace. This process may be carried on a time and space window basis.
We introduced a modified L_1 norm, which focus on the minimization of positive residuals and leads to a stable estimation of the spectrum envelope. Synthetic and real data examples show that this new norm provide a superior estimation of the residual seismic pulse when compared to the wavelets estimated using the L_2 norm.

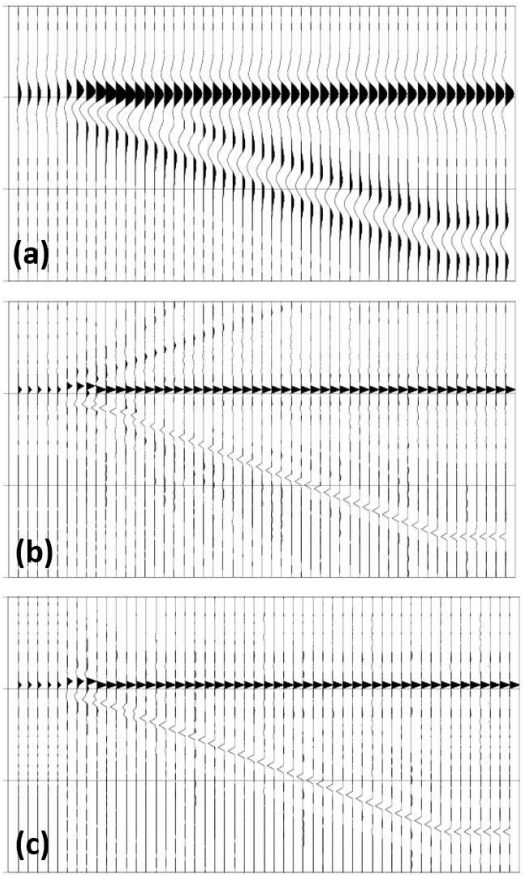

Figure 9: (a) Synthetic wedge model data; (b) sparse deconvolution with L_2 norm wavelet estimation; (c) sparse deconvolution with the modified L_1 norm wavelet estimation.

Acknowledgments

The author would like to thank Petrobras for the permission to publish this work and Andre R. Rosa for setting the basis from which the present work evolved.

References

Portniaguine, O., and Castagna, J. P., 2005, Spectral inversion: Lessons from modeling and Boonesville case study: 75th Annual International Meeting, SEG, Expanded Abstracts, 24, 1638-1641.
Rosa, A. R., 2010, Análise do Sinal Sísmico, Sociedade Brasileira de Geofísica.
Rosa, A. R., and Ulrych, T. J., 1991, Processing via spectral modeling: GEOPHYSICS, 56; P. 1244-1251.
Zhou, H., Wang, Y., Lin, T., Li, F., and Marfurt, K. J., 2015, Value of nostationary wavelet spectral balancing in mapping a faulted fluvial system, Bohai Gulf, China: Interpretation, v. 3, P. SS1-SS13.

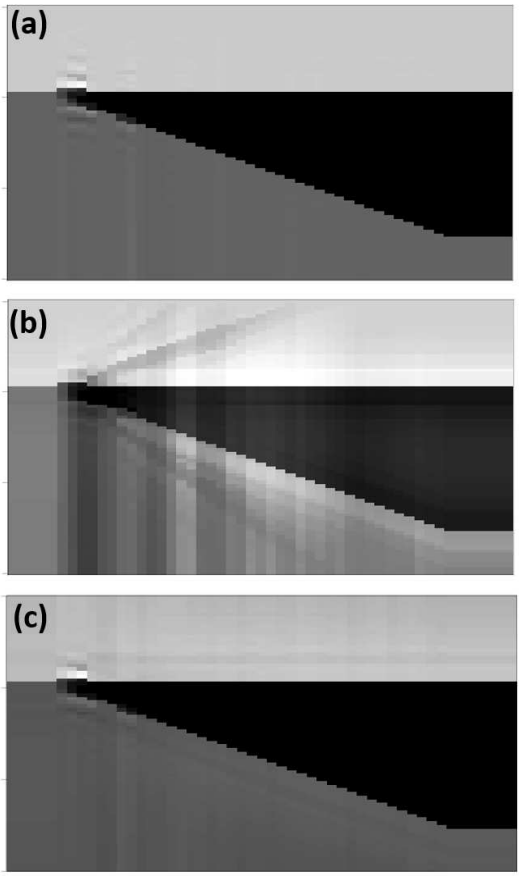

Figure 10: Retrieved impedance from deconvolution with: (a) the true wavelet; (b) the L_2 norm wavelet; (c) the L_1 norm wavelet.

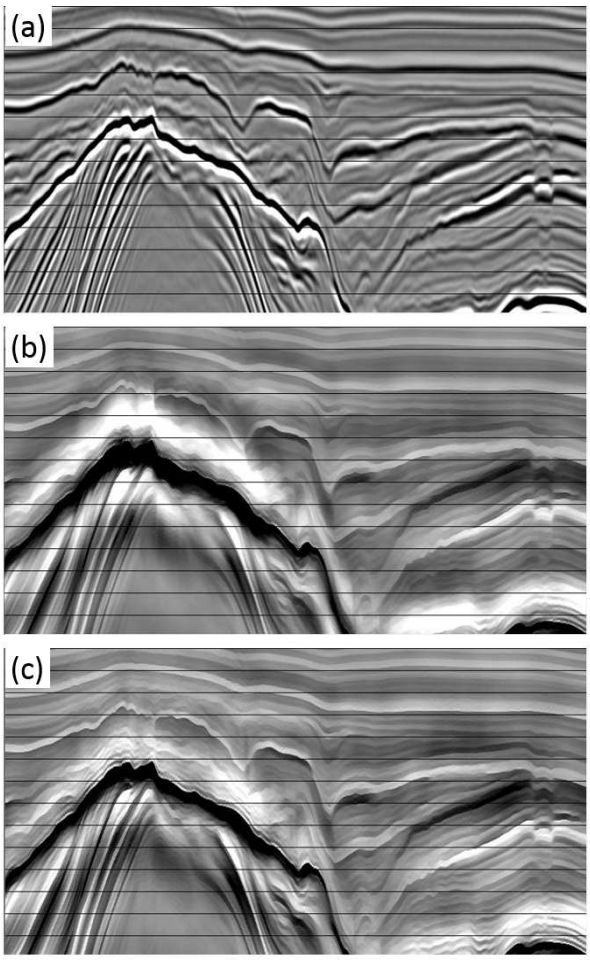

Figure 11: Real data example: (a) amplitude data; (b) band-limited impedance with L_2 norm wavelet; (c) band-limited impedance with L_1 norm wavelet.

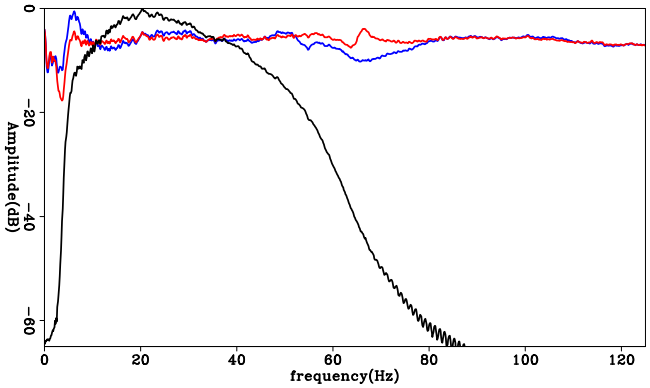

Figure 12: Spectra from Figure 11: amplitude data (black); reflectivity with L_2 norm wavelet (blue); reflectivity with L_1 norm wavelet (red).